Synchronous Operation of High Frequency Inductive Power Transfer Systems through Injection Locking

Nunzio Pucci, *Student Member, IEEE,* Christos Papavassiliou, *Senior Member, IEEE,* and Paul D. Mitcheson, *Senior Member, IEEE*

***Abstract*—High frequency inductive power transfer systems can be designed for operation with high tolerance to misalignment and large air-gaps, making it possible to operate in highly dynamic environments. Most examples in the literature use a single active transmitter and a single passive receiver (active-passive approach). Such systems are limited to unidirectional power flow and are susceptible to detuning of the transmitter due to changes of reflected reactance stemming from diode non-linearities. This also limits the range of coupling over which the system can be operated efficiently. Therefore there is significant potential for expanding the range of applications of inductive power transfer systems by moving to an active-active configuration. This will enable bidirectional power flow, power routing through several nodes and on-the-fly retuning to eliminate reflected reactances. One of the greatest challenges in achieving an active secondary in an IPT system is obtaining a stable frequency and phase reference for the synchronous rectifier/transceiver with respect to the transmitter coil current and hence magnetic field. Various methods for synchronisation have been proposed in the literature, but they either require a separate, out of band communication link, or are difficult to scale to MHz operation. This paper describes an alternative to the existing solutions, using an injection locked oscillator to provide optimal phase tracking. A series of candidate feedback configurations are also proposed to provide high system resilience. In this work the basic principles of injection locking are described as applied to synchronous IPT transceivers and experimental results are presented demonstrating its application to a bidirectional back-to-back Class-EF configuration operating at 13.56 MHz, with coupling factors ranging from 1.9 % to 8.4 % and power levels of up to 25 W.**

***Index Terms*—Class EF, resonant power converter, high frequency, wireless power transfer, synchronous rectification, injection locking**

I. Introduction

INDUCTIVE power transfer (IPT) has been an extensively growing topic of research in the past two decades. With the development of wide-bandgap devices, it has been possible to extend the possible frequency of operation to the Megahertz range for moderate power levels. Increasingly refined designs have been proposed to address challenges such as efficiency, coil separation distances and misalignment tolerance, leading to a higher number of applications for which IPT is a feasible solution, both in the kilohertz and the Megahertz range.

A. Bidirectional Power Transfer and Power Routing

Whilst most of the literature to date presents designs that are restricted to unidirectional power flow from a single transmitting inverter to a single passive receiver rectifier (active-passive systems), operation of bidirectional systems has become a topic of increased interest [1]. Reversible power flow capability, enabled through synchronous operation of both sides of the wireless link (active-active systems), opens up new opportunities for IPT in applications such as vehicle-to-grid [2]–[4] and drone-rechargeable sensor networks [5].

Furthermore, the possibility of controlling the phase of the current in each transceiver coil for a fixed frequency reference can be used to enable applications where multiple nodes of an IPT system cooperate to route power and shape the magnetic field around the system. Applications that involve a network of cooperative and re-configurable transceivers can be beneficial in highly automated environments, such as factories, aerospace, or other applications where human intervention is limited.

In addition, due to the ability for an active-active system to self-tune, operation down to very low coupling factors, and hence applications which demand large air-gaps, is possible.

B. Benefits of Synchronous Rectification at Low Coupling

High frequency inductive power transfer (HF-IPT) systems typically use air-core coils to achieve an unconstrained magnetic flux, hence making it easier to achieve efficient transfer of power [6]–[9] for large distances and with a large tolerance to misalignment [10], [11]. The work in [12]–[17] shows that it is even possible to design such systems for a large tolerance to load variations.

While it is possible to achieve high efficiency under a large set of operating conditions there are still existing constraints in the development of HF-IPT systems: passive rectifiers are typically a common choice because of their simplicity and achievable efficiency, however the characteristics of their reflected impedance back to the primary can be heavily affected by the magnitude of the induced voltage of the secondary (as shown in [18], [19] because of the non-linear diode capacitance), hence making it more challenging to tune a system for this wide range of operating conditions. In addition, low coupling operation can lead to extra losses: the induced voltage in the secondary coil reduces with a decrease in coupling factor. For a fixed power level it is then necessary to have larger currents, increasing the losses when employing a passive rectifier due to the constant voltage drop across the diodes.

Synchronous rectification addresses both of these issues: the voltage drop across a conducting transistor is typically small

compared to the voltage drop across a diode, hence the losses would be lower. In a synchronous rectifier it is also possible to control the phase between primary and secondary, hence making it possible to track a state of zero-reflected-reactance for optimal operation as the coupling changes.

In [20] a performance comparison between an active-passive and active-active configuration for Megahertz IPT system is provided, proving that even for frequencies as high as $27.12\,\mathrm{MHz}$ a synchronous rectifier can be advantageous in terms of end-to-end efficiency.

C. Challenges in Transceiver Synchronisation at Megahertz

One of the main challenges in operating a synchronous or a bidirectional HF-IPT system is clock synchronisation of the two sides of the system: if there is a frequency mismatch between primary and secondary, it is not possible to operate under a fixed relative phase. To transmit real power between primary and secondary, a fixed phase close to $\pm 90^\circ$ is required so that the induced voltage and the current in the secondary resonator are in phase (i.e., no reflected reactance). If a constant phase slip is introduced between the currents in the primary and secondary as a result of a frequency mismatch between the two sides, it will result in an average power transmission of zero.

Solutions for synchronisation have been proposed for low frequency [2], [4], [21] and high frequency [12], [22], [23] active systems. Nevertheless, some of them are difficult to apply to Class EF-based HF-IPT systems because of the circuit configuration [21] and/or the required instrumentation bandwidth for a high frequency counterpart [2], [4]. The work presented in [22] requires an additional coil to measure the current, which is feasible for applications at this frequency range, but it introduces additional elements in the inverter, hence leading to a potential alteration in the topology of the resonant link because of parasitics. In [12] the authors propose a method that only works in specific conditions: the system will operate for a fixed on-time to achieve zero-voltage switching, but the off-time will change. This means that the system is effectively performing a dynamic frequency tuning with variable relative duty cycle. This can sometimes lead to instability. In [23] the authors use an auxiliary communication link.

This paper presents a possible alternative to tackle some of the difficulties highlighted above: a separate communication link is not required, it is not necessary to carry out complicated signal processing tasks, and the proposed method allows operation under extremely low coupling conditions. This is achieved using an injection locked oscillator, hence making it possible for the secondary side of the system to naturally converge to the operating frequency of the primary at a fixed relative phase offset.

It is illustrated how this can also be used in conjunction with other techniques to track and correct the optimal phase and achieve closed loop control of the system. Experimental results show the start-up behaviour of the system, the effect of temperature on the oscillator's behaviour and stable system operation for different operating conditions, with power levels of up to 25.7 W.

This paper is organised as follows: Section II provides an overview of Class EF transceivers, and how they are operated for bidirectional power transfer. Section III describes the basic principles of injection locking, and how this can be used in a HF-IPT system to achieve synchronous rectification. Section IV presents the experimental results obtained by operating a bidirectional 13.56 MHz IPT system based on a back-to-back Class EF configuration. Section V explains how it is possible to implement a closed loop configuration to improve the reliability of the system for different operating conditions. Section VI concludes the paper.

II. Implementing Class EF Transceivers for Bidirectional Wireless Power Transfer

The Class EF topology, shown in Fig. 1 in a back-to-back bidirectional configuration, is a coil driver which is often employed in IPT systems operating in the Megahertz range. This topology comprises just a single low-side switch, making it easy to drive, and is typically operated in open loop with a fixed frequency and duty cycle. The Class EF shares multiple similarities with a Class E coil driver, but the addition of an extra LC branch makes it possible to obtain an extra degree of freedom in the design. This can be used to shape the drain waveform, lowering its peak voltage (hence reducing the stress on the device) or to achieve desirable system properties such as load independence [12] by relaxing design constraints exclusively to zero-voltage-switching (ZVS).

In the specific context of this work, the Class EF load independent topology is useful because it introduces additional system tolerance in terms of load variations, which can be beneficial either when the coupling changes, or when the phase-search algorithm is being performed, ensuring safe transceivers operation for a wide range of loading scenarios.

As shown in [12], [24], [25], this topology can be arbitrarily used as an inverter or a rectifier, with the only difference being the relative phase between transmitter and receiver coil currents: keeping this phase at $\pm 90^\circ$ ensures operation of each side of the system as transceivers capable of exchanging power with no reflected reactance.

TABLE I
Components values for Transceiver A and Transceiver B. Class EF transceivers, $V_{dc} = 60\,V$, $\delta = 30\,\%$, planar PCB coils from [26] on both sides.

Component	Transceiver A	Transceiver B	Description
C_1 (pF)	100+C_{oss}	92+C_{oss}	Vishay QUAD HIFREQ
C_2 (pF)	186	200	Vishay QUAD HIFREQ
C_3 (pF)	125	136	Vishay QUAD HIFREQ
L_1 (µH)	88	88	Wurth Elektronik WE-PD
L_2 (nH)	234	251	Coilcraft 2014VS
L_3 (nH)	1181	1181	IPT PCB coils
Q_1			GS66504B (650 V, 15 A) GaN FET

The component values used in this work for Transceiver A and Transceiver B (Fig. 1) are reported in Table I. The two sides are both tuned to achieve load independence, although the exact component values are slightly different due to parts shortage. Further details on how to select components and

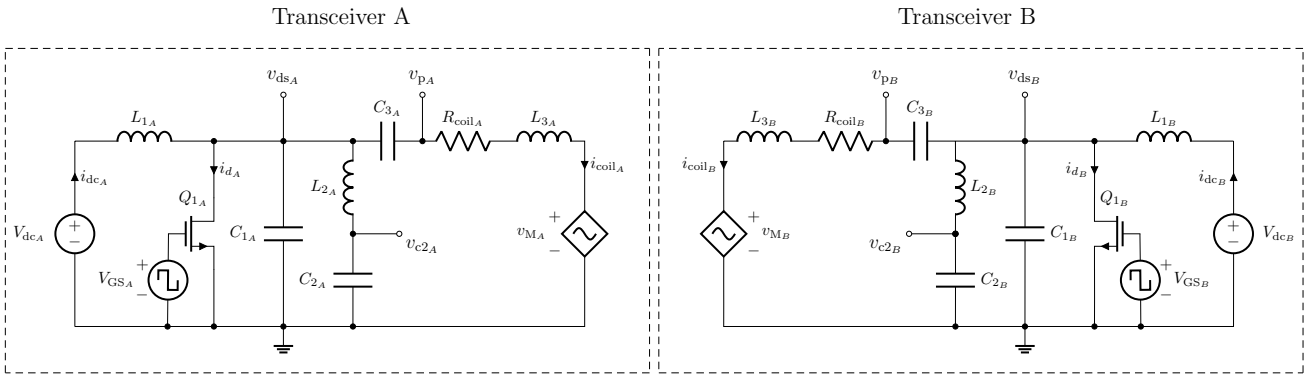

Fig. 1. Circuit diagram of two bidirectional Class EF transceivers with the loads modelled as dependent voltage sources.

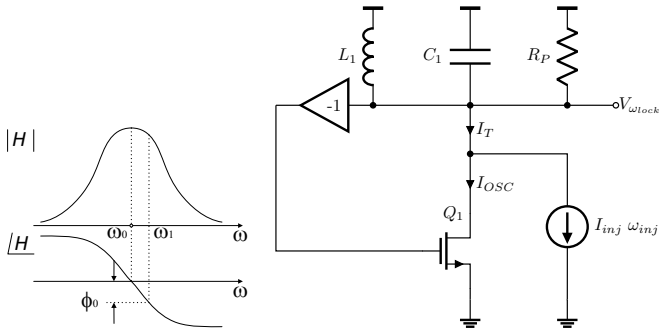

(a) Phase offset of an oscillator that is being pulled. (b) Conceptual circuit diagram of an oscillator under injection.

Fig. 2. Injection locked oscillator conceptual diagrams [29].

system parameters (such as duty cycle and input voltage) for the Class EF load independent topology are reported in [12].

In this work the transceivers are operated at a frequency of $13.56\,\mathrm{MHz}$ to exploit the improvement in quality factor of air-core coils in the Megahertz range, hence achieving an unconstrained magnetic flux, which can be useful to achieve efficient operation for larger distances and with larger tolerance to misalignment. Other Megahertz ISM band frequencies (such as $6.78\,\mathrm{MHz}$) could also be used with these coils.

III. Basic Principles of Injection Locking

Injection locking is a phenomenon that has been studied since 1946 [27]–[31]. The core idea of injection locking is that under some specific circumstances, it is possible to synchronise the frequency of two independent oscillators, provided that coupling between two oscillators is present and the natural oscillating frequencies of the oscillators are somewhat close (i.e., operating within the lock range as per Equation 5).

If the coupling between an oscillator with a natural oscillating frequency of ω_0 (slave side) and an oscillator with a natural oscillating frequency of ω_1 (master side) is sufficient to overcome the difference $\omega_0 - \omega_1$, it is possible to pull the oscillator from a frequency of ω_0 to a frequency of ω_1. This comes with an inherent phase offset which depends on quality factor and frequency difference as explained in [29] and summarised in Fig. 2, where I_{osc} is the current present in the feedback loop of the oscillator that is being injection locked and I_{inj} is the current pulled from the feedback loop of the oscillator as a consequence of the coupling with the system operating at a frequency of ω_1.

The lock range of an oscillator ω_L can be obtained as shown in [29]. A second order resonant tank like the one illustrated in Fig. 2 exhibits a phase shift α when oscillating at a frequency ω_1, in vicinity of its resonance ω_0:

$$\alpha = \frac{\pi}{2} - \tan^{-1}\left(\frac{L_1\omega_1}{R_P}\cdot\frac{\omega_0^2}{\omega_0^2-\omega_1^2}\right) \tag{1}$$

It is possible to approximate $\omega_0^2 - \omega_1^2 \approx 2\omega_0(\omega_0-\omega_1)$ and rewrite $L_1\omega_1/R_P = 1/Q$ and $\pi/2 - \tan^{-1}x = \tan^{-1}(x^{-1})$:

$$\tan\alpha \approx \frac{2Q}{\omega_0}(\omega_0-\omega_1) \tag{2}$$

When the oscillator experiences the effect of the injection current I_{inj}, I_{inj} and I_{OSC} will exhibit an angle of $\phi_1+\phi_2$, with ϕ_1 being the angle between I_{inj} and I_T and ϕ_2 being the angle between I_T and I_{OSC}. When ω_{inj} (or ω_1) departs from ω_0 the phase shift introduced by the tank increases together with the angle ϕ_2. This implies a counterclockwise rotation of I_{OSC}. It is possible to write:

$$\sin\phi_2 = \frac{I_{inj}}{I_T}\sin\phi_1 = \frac{I_{inj}\sin\phi_1}{\sqrt{I_{OSC}^2 + I_{inj}^2 + 2I_{OSC}I_{inj}\cos\phi_1}} \tag{3}$$

To find the lock range this expression is maximised, leading to $\sin\phi_{2,\max} = I_{inj}/I_{OSC}$ when $\cos\phi_1 = -I_{inj}/I_{OSC}$. This translates in an angle of $90°$ between I_{inj} and I_T. Hence it is possible to write $\tan\phi_2 = I_{inj}/I_T$ and $I_T = \sqrt{I_{OSC}^2 - I_{inj}^2}$.

Using this information in conjunction with Equation 2 (setting $\alpha = \phi_2$) it is possible to write:

$$\omega_L = \omega_0 - \omega_1 = \frac{\omega_0}{2Q}\cdot\frac{I_{inj}}{I_{OSC}}\cdot\frac{1}{\sqrt{1-\frac{I_{inj}^2}{I_{OSC}^2}}} \tag{4}$$

When approaching the edge of the lock range (i.e., $I_{inj} \ll I_{OSC}$), this is approximately:

$$\omega_L \approx \frac{\omega_0}{2Q} \cdot \frac{I_{inj}}{I_{osc}}, \tag{5}$$

Further details of this derivation are provided in [29].

This property can be advantageous, especially in the context of synchronous rectification, where a switching signal needs to be generated in quadrature with that of a master. Changing the natural oscillating frequency of such an oscillator can hence serve two purposes: facilitate injection locking over a wider range, or provide a set phase offset. As will be discussed in Section V, the way the phase offset is controlled, either by changing ω_0 or introducing an external delay, depends on the circumstances.

From (5) it is clear that to maximise ω_L, it is necessary to have a large magnitude of I_{inj}, especially when trying to pull an oscillator with a high quality factor. As reported by [29], the non-linearity of the oscillator is another key component, as a perfectly linear oscillator with a high quality factor would not be pulled by the means of injection locking.

Failure in synchronisation was monitored with the experimental setup for distances between primary and secondary coils of more than $35\,\mathrm{cm}$ (almost two coil diameters): the system entered quasi-locking, showing a characteristic phase slip at regular intervals of around half a second. For distances higher than $40\,\mathrm{cm}$ frequency locking is lost completely, implying that the system is operating well beyond the established lock range ω_L. An example of typical phase slip behaviour caused by quasi-locking is reported in [29], Fig. 7.

We have observed injection locking occurs even when lowering the input voltage of the two transceivers to around 10 V, with corresponding coil currents of around 500 mA, but no useful exchange of power (i.e., the losses were higher than the transferred power, but the coil currents were synchronised).

The lock range is dependent on the magnitude of the injection current (see Equation 5), and hence the separation between the two sides of the system. For a coil separation of $25\,\mathrm{cm}$, the lock range of the oscillator is estimated to be around $60\,\mathrm{kHz}$. Using the ring-down method, the quality factor of the oscillator in Fig. 3 is estimated to be around 86, with a corresponding $I_{\mathrm{OSC}} = 1\,\mathrm{mA}$.

One matter that arises from employing injection locking in an HF-IPT systems is the possibility of simply synchronising independent crystals using the same principle. While this is possible in theory, this task can prove rather challenging in practice: the high quality factor of the crystals, together with a relatively small packaging which minimises the coupling with the injection current make it difficult to simply synchronise the two sides of the system without using a dedicated oscillator that has been specifically designed for the task. In this work this task is attempted using the experimental setup of Section IV. Even when placing the coil of the master side directly above the crystal of the slave side, our attempts at pulling an independent SG-210 STF CMOS oscillator proved unsuccessful.

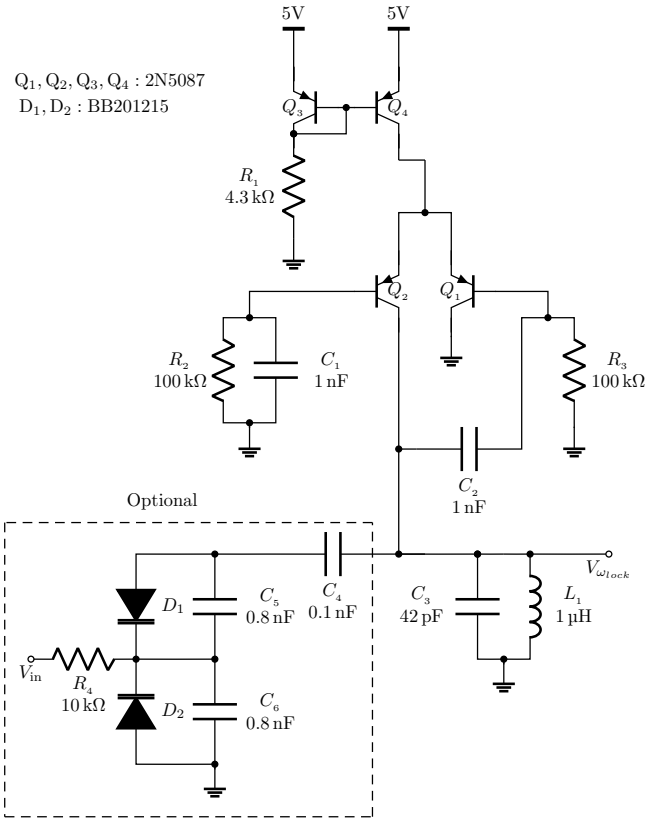

(a) Complete schematic of the injection locked oscillator. The optional dashed elements are used to control the resonant frequency with a given input voltage.

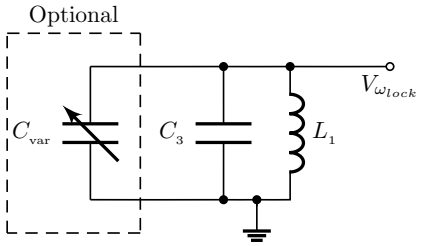

(b) Resonant tank of (a) including the varactor diodes as an equivalent variable capacitance.

Fig. 3. Circuit diagrams of the oscillator.

IV. System Design and Experimental Results

The system (shown in Fig. 4) consists of two back-to-back Class EF transceivers connected as shown in [25] and Fig. 1: the input voltage of each of the two sides of the system is provided through a source-sink configuration of an electronic load in constant voltage mode (the sink) operated in parallel with a power supply (the source). This makes it possible to obtain the same input voltage for each side of the system, while enabling the possibility of bidirectional operation.

The link consists of two PCB planar coils (two-turns, with an external diameter of $20\,\mathrm{cm}$), with an inductance of $1.18\,\mu\mathrm{H}$ and a quality factor of more than 500 at $13.56\,\mathrm{MHz}$. More details on coils design and characterisation are reported in [26], [32]. These coils are chosen for ease of reproducing the experiment and accurately controlling the separation between the coils. In this work the variations in coupling factor are achieved solely by changing the distance between the two coils (z-direction), but it is in principle possible to replicate the same results through the choice of an appropriate misalignment in the x-direction and y-direction.

This article has been accepted for publication in IEEE Transactions on Power Electronics. This is the author's version which has not been fully edited and content may change prior to final publication. Citation information: DOI 10.1109/TPEL.2023.3300510

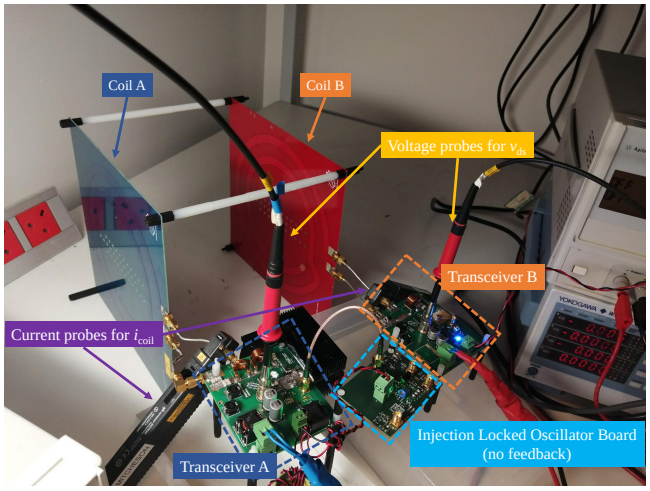

Fig. 4. The experimental setup.

Table I summarises the components for the two transceivers. One of the two sides of the system (the master) uses a crystal oscillator to generate V_{GS}, while the other side (the slave) uses the oscillator in Fig. 3 to match the frequency of the master through injection locking as explained in Section III. This works similarly to a pMOS differential LC oscillator, with the only difference being that one of the two sides of the tank is grounded. The optional circuitry presented in Fig. 3 can be used to control the natural oscillating frequency of the injection locked oscillator. Effectively, the varactors act as a variable capacitance to control the resonant frequency of the tank through an input voltage V_{in}.

This makes it easier to injection lock to the master by bringing the natural frequency of the oscillator closer to that of the crystal on the master, or producing a controlled phase offset of V_{GS} on the slave side.

If the latter makes it unfeasible to achieve injection locking because the slave side is being pushed into quasi-locking, or if the system is being operated without the optional circuitry, it is possible to use a delay module at the output of the oscillator to change the phase of V_{GS} relative to the transmit coil current without affecting the natural frequency of the oscillator. This has been verified experimentally using a DS1023-50 delay module. The stage before the gate drive is always a monostable circuit to make sure that the duty cycle is fixed at 30 %.

The system is designed by setting a resonant tank frequency through a selection of $C_{3,4,5,6}$ and L_1. This combination is set to ensure a change in resonant frequency from 13.5 MHz to 13.6 MHz with a corresponding change in V_{in} from 0 V to 5 V as a consequence of the change in capacitance of the varactors $D_{1,2}$.

The circuit in Fig. 3 works as follows: the injected signal is an additive emf to the voltage developed on L_1 . The two are fed back through the high pass filter $C_2 - R_3$ to Q_1 which is non-linear, so it generates a pulse current sequence at the collector of Q_1 . As the sum of the collector currents of Q_1 and Q_2 is constant, the pulse sequence, but of opposite sign is applied to the tank $L_1 - C_3$. A detailed explanation of the pulling and locking mechanism has been given in [31].

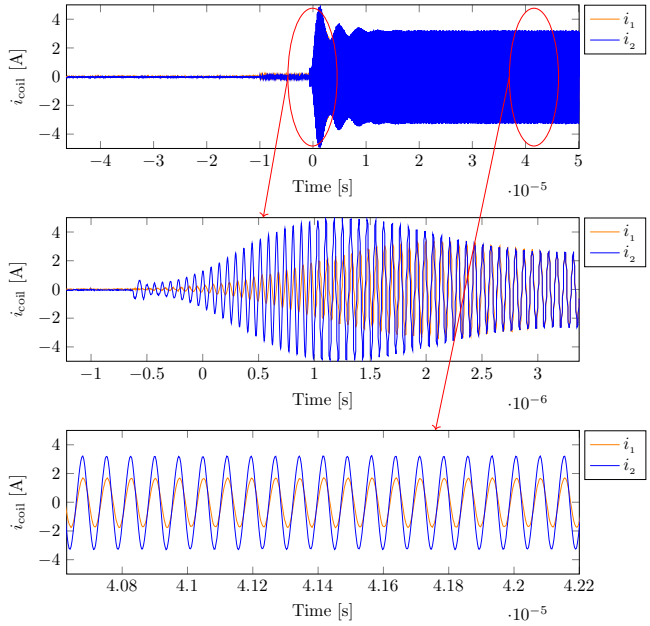

Fig. 5. Coils currents when starting up the system: master in blue, slave (operated by the injection locked oscillator) in orange. The three figures show details at different time points.

The system is operated at a frequency of 13.56 MHz for a fixed input voltage of 60 V at both sides, and with a fixed duty cycle of 30 %.

When both sides of the system are simultaneously switched on, the master will start producing a coil current at the frequency of its crystal oscillator. After a couple of cycles, the magnetic field generated by this current will be large enough to pull the oscillator circuit on the slave side to the frequency of the master, which will then stabilise its frequency and phase, hence reaching steady-state. For practicality, it is assumed that both sides have enough energy to bootstrap the system. In actual facts it does not matter which side of the system is turned on first or whether the master resides with the transmitter or the receiver.

This process is summarised in Fig. 5, in which the details of the coil currents in each of the two sides of the system are shown, with the master in blue and the slave in orange. In this specific scenario the system has been set up to have a phase offset of zero to facilitate the visualisation of a successful phase lock, but in practice it will typically be operated with a phase offset between primary and secondary coil currents of $\pm 90°$. Frequency and phase lock occur after a transient of less than 30 µs.

While in this work a dedicated coil to synchronise the slave side oscillator is not present, it is in principle possible to add this element to facilitate the process of injection locking. In this work the unconstrained magnetic field from the link can generate the required injection current on the oscillator board without the need of additional elements.

Fig. 6 shows a scope capture of the system operating with the required phase offset of $\pm 90°$ for optimal power transfer efficiency. The coil currents (top waveforms) show that the required phase offset is achieved. The reported drain voltage

This article has been accepted for publication in IEEE Transactions on Power Electronics. This is the author's version which has not been fully edited and content may change prior to final publication. Citation information: DOI 10.1109/TPEL.2023.3300510

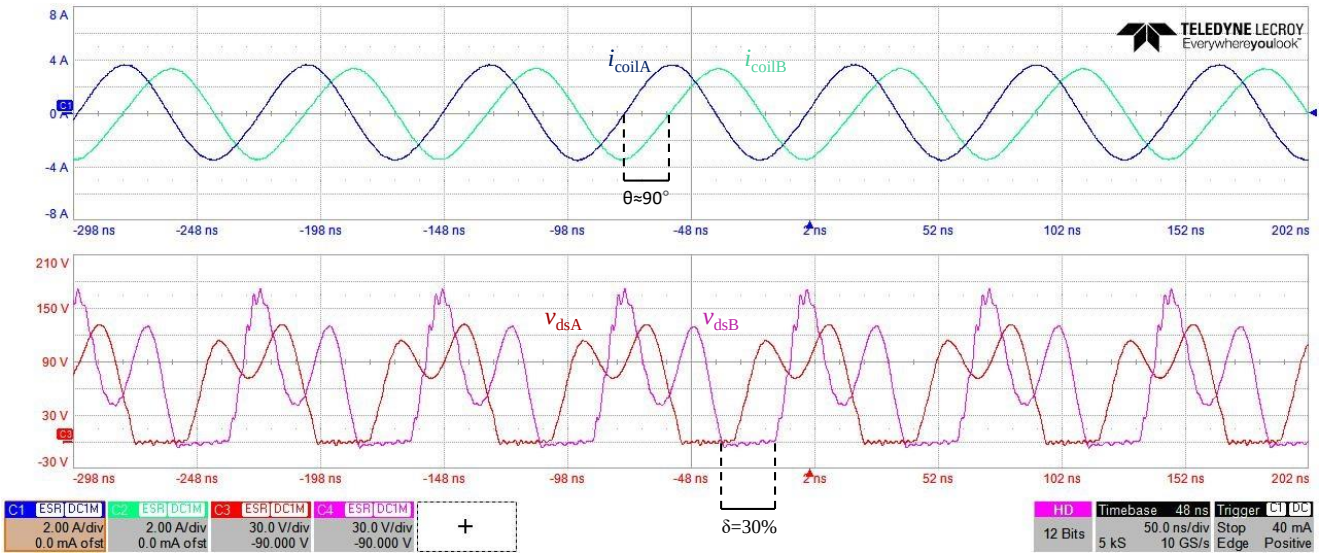

Fig. 6. Scope capture of the system operating under injection locking. Coils currents on the top, drain voltage waveforms on the bottom.

waveforms on the bottom show soft switching is achieved in both transmitter and receiver side.

As reported in [33], it is possible to exploit the phenomenon of injection locking even with passive rectifiers, so that the frequency of the primary matches the resonant frequency of the secondary for optimal power transfer efficiency. Similarly, in the proposed system, when the input voltage of the master side is forced to short or open, the injection locked oscillator on the slave side will still manage to match the frequency of the current circulating in the primary coil, provided that the transistor on the master side is still switching at the desired frequency: if there is a small excitation current on the master side coil, this will propagate an injection current at the correct frequency in the oscillator of the slave side, stabilising both sides of the system at a matched frequency.

When the system is operated without a master side in proximity, the oscillator will just oscillate at its natural frequency and the transceiver will still work correctly, since the natural frequency of the oscillator is designed to be relatively close to that of the operating system.

TABLE II
SYSTEM OPERATION FOR DIFFERENT COILS SEPARATIONS

Distance [cm]	k [%]	Phase [°]	I/P Power [W]	O/P Power [W]	$\eta_{\mathrm{DC-DC}}$ [%]
30	1.2	89	12.1	0.9	0
25	1.9	89	14.4	-3.2	22.2
20	3.1	88	20.6	-9.2	44.7
17.5	4.5	90	25.5	-13.7	53.7

Table II shows input and output power for different operating conditions.It is possible to reliably transfer power down to a coupling of 1.9 %, and synchronisation is not lost until the coupling is lower than 0.9 % (35 cm separation). For a coupling of 4.5 % it is possible to transfer 13.7 W with a 53.7 % end-to-end efficiency. For higher coupling and power levels these figures tend to be higher: the standby power of the design implemented in this work is around 4 W per side. The efficiency is measured by monitoring the power at both ends of the system using a Yokogawa WT332E Digital Power Meter.

Low-efficiency/low-coupling scenarios have been specifically addressed to further validate the applicability of the proposed approach under difficult conditions.

A breakdown of the losses for the 4.5 % coupling scenario is presented in Fig. 8.

A crucial task to operate this type of system reliably for any given external environment is the design of a feedback loop. While the previous section demonstrated system operation in open loop, there is a wide range of factors that can affect the operation of the system, leading to possible sub-optimal operation or even failure of the system as a whole.

Temperature is one of the main factors that changes over time and can impact the operation of the system: as shown in Fig. 7, the oscillator module's operating temperature can change by up to 10 °C in a controlled environment (even more when deployed in the field). This can affect the operation of the semiconductor devices used in the oscillator, even leading to changes in the natural frequency of oscillation (and the lock range as per Equation 5). The consequences of this can range from an unwanted injection of phase to complete loss of synchronisation: as explained in Section III as the natural frequency of the oscillator gets further apart from that of the master side, the phase will change. Also, the required magnitude of the injection current will grow larger.

In Fig. 10 it is possible to observe how over a time span of 10 minutes the temperature has gone up by almost 10 °C, and the phase has gone down by 30°. This is something to avoid in an operating system. A closed loop feedback system can mitigate this problem.

V. CLOSED LOOP OPERATION

The method described in [34], which consists of a technique to estimate the reflected impedance in a Class EF system, could be implemented to solve this issue: a reference voltage

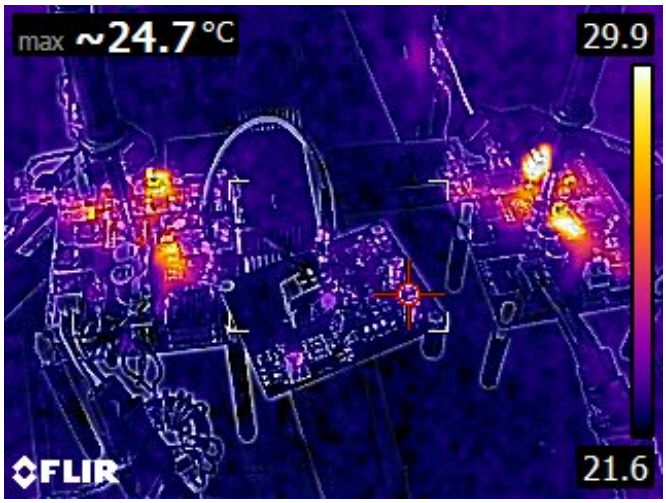

(a) Temperature of the oscillator module before operation.

(b) Temperature of the oscillator module approaching steady state.

Fig. 7. Thermal camera pictures of the system with focus on the injection locked oscillator module.

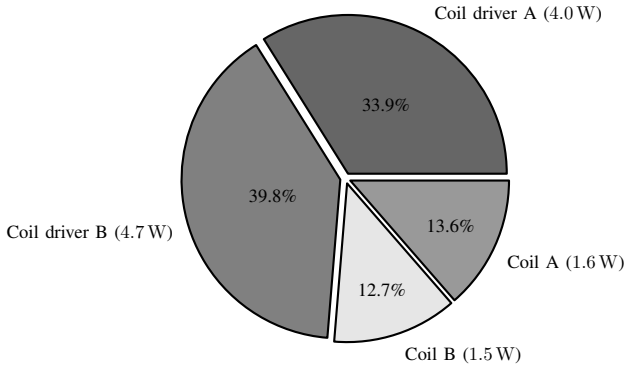

Fig. 8. Distribution of losses with a coupling factor of 4.5 %

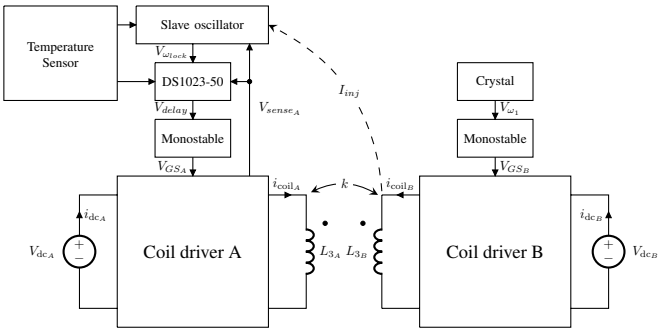

Fig. 9. Block diagram of the system feedback loop.

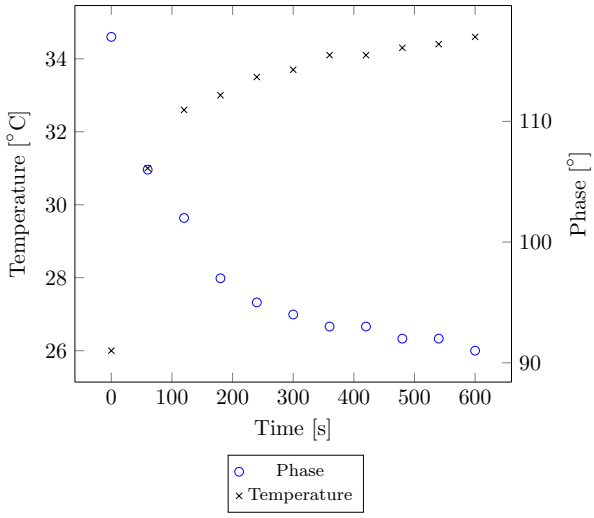

Fig. 10. Temperature dependence of coils currents relative phases over time.

level would be provided to monitor the reflected reactance and the relative phase offset could then be adjusted accordingly. However there is a practical consideration to make: this method is based on the extraction of information at a single frequency, but the system presented in this paper has an oscillator with a frequency that might change during the adjustment in the feedback loop or when synchronisation is lost.

Designing the same system with filters that have a wider bandwidth would solve part of the problem, but the required filter transfer function would need to be extremely flat over the operating frequency range. It has been observed experimentally that this method works when the system is already in a stable state, and hence the frequency remains fixed, but it would be otherwise impossible to use the reflected impedance estimation technique to lock the oscillator when starting the system from an unstable state: two slightly different operating frequencies can lead to the same reference voltage value for the reflected impedance estimation as a consequence of the filters response not being constant over the operating range.

A simpler alternative is to perform phase control (or natural oscillating frequency control) of the slave oscillator through a direct measurement of the factors that may affect injection locking. While temperature is possibly one of the easiest to observe, other factors can be ambient EMI, humidity, light

This article has been accepted for publication in IEEE Transactions on Power Electronics. This is the author's version which has not been fully edited and content may change prior to final publication. Citation information: DOI 10.1109/TPEL.2023.3300510

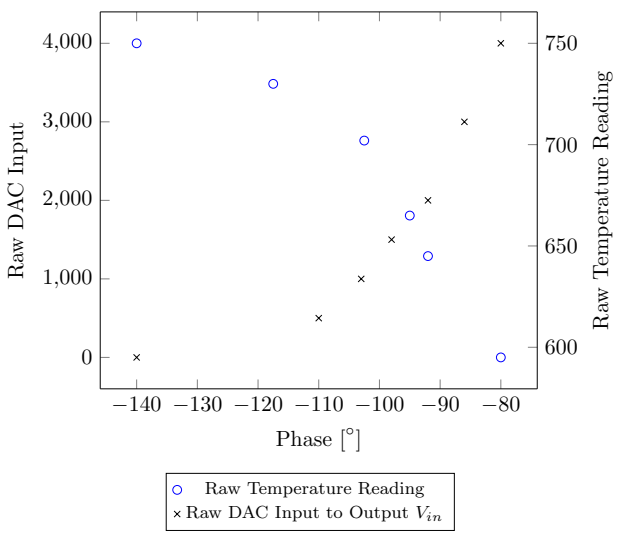

Fig. 11. Phase between coil currents as a function of raw temperature reading from PT100 and raw input of the ADC to output V_{in}.

and radiation. In this work the feedback loop is only based on temperature, but it is in principle possible to monitor the other aforementioned factors employing appropriate sensors. This correction can be done as shown in Fig. 9 using a lookup table to perform the desired correction to either the oscillating frequency or the phase.

It is known from Section III that affecting the natural oscillating frequency of the oscillator will also affect the phase at which injection locking occurs, but it will also change the locking range (as reported in (5)). This implies that in some scenarios where all the corrections are applied through the input voltage V_{in} of the VCO in Fig. 3, the lock range could be decreased to a critical level that would prevent injection locking.

For this reason the only adjustments that should be performed through V_{in} are the ones to counteract the change in natural oscillating frequency of the oscillator (such as temperature). Other corrections applied to account exclusively for a shift in phase, but not oscillating frequency, (i.e., fine tuning of the system or changes in reflected reactance from a coupled resonant circuit) should be performed through the delay module, so that the optimised locking range remains unaffected.

This allows operation of the system for relatively stable values of ω_0 and ω_L, hence providing higher rejection of disturbances from external sources, improving the resilience of the system.

The feedback to provide the required adjustments of ω_0 in response to temperature variation is designed by characterising the produced phase offset between coil currents as an effect of a variation in the voltage across the varicap diodes (V_{in}) and as an effect of the temperature in proximity of the custom oscillator of Fig. 3 using a PT100 temperature sensor. Using a combination of these two experimentally derived relationships (shown in Fig. 11) it is possible to create a lookup table to correct the phase offset produced by the temperature variation by changing the value of V_{in}, and hence ω_0 and the phase between the coil currents.

An additional step to improve the resilience of the system is an extra feedback loop to perform phase correction through the delay module in response to possible detuning of the system. This can be done using a maximum power point (MPP) tracking algorithm to maximise the power received by the slave side of the system. Since the input voltage of the transceivers is constant in this design, the received power is estimated using the receiver current, which is measured using a current sensor. The phase between coil currents will converge to a value close to $-90°$ for minimum reflected reactance on the receive side and maximum received power as explained in [23]. Bidirectional power transfer can be achieved by simply introducing a phase offset of π using the delay module.

The synchronisation process is summarised as follows:

1) Read the temperature to obtain a value for the estimated phase shift solely as a result of the temperature change (i.e., phase difference because of pre-characterised temperature-phase relationship from Fig. 13).
2) Change the input voltage of the VCO according to the pre-characterised DAC input-to-phase relationship to counteract possible changes in oscillator's natural frequency based on the estimated phase difference from the temperature reading. These two steps can be merged using a look-up table to directly translate a temperature reading into a microprocessor output to the DAC: for example if the temperature reading indicates an estimated phase that is $30°$ lower than expected, the DAC will produce the corresponding VCO voltage value to introduce a $30°$ phase shift in the opposite direction. For this reason the DAC is initially set to a value with equal headroom and legroom to produce the required corrections. This is done using the data in Fig. 13 and performing interpolation for the intermediate points.
3) Start introducing phase changes through the delay line and find the point at which the received power is the highest.
4) Convergence is achieved.
5) Keep monitoring the temperature and correct the input voltage of the VCO at regular intervals to prevent phase injection from temperature changes.
6) Keep the two points adjacent to the current operating point for maximum received power and adjust the delay line accordingly.
7) Repeat steps 5 and 6 to ensure the appropriate phase is maintained.
8) (Optional) Add a further phase shift of π if the direction of the system power flow needs to be reconfigured.

It is still possible that the transmitter will operate sub-optimally under these circumstances as a result of possible tuning mismatches between the two sides: the transmitter can still operate under non-zero reflected reactance as shown in Fig. 12. In this experiment the system has been purposely pushed above the power level for which it was designed. From Fig. 12 it is in fact possible to observe that while the receiver's drain voltage waveform is soft-switching as expected, the

This article has been accepted for publication in IEEE Transactions on Power Electronics. This is the author's version which has not been fully edited and content may change prior to final publication. Citation information: DOI 10.1109/TPEL.2023.3300510

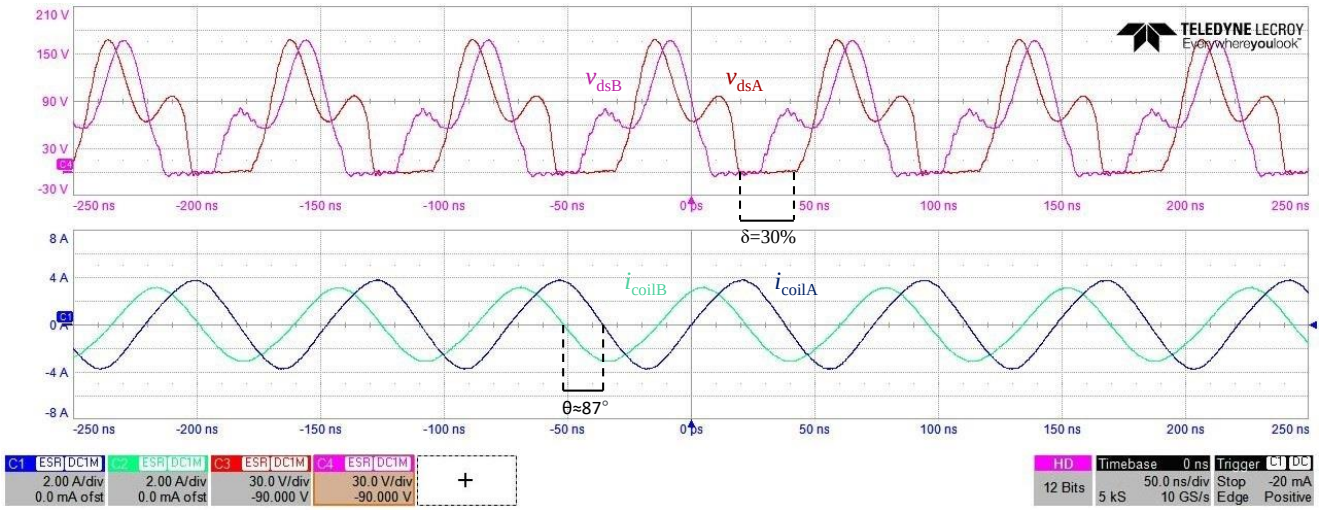

Fig. 12. Scope capture of the system operating under injection locking with feedback loop. Coils currents on the bottom, drain voltage waveforms on the top.

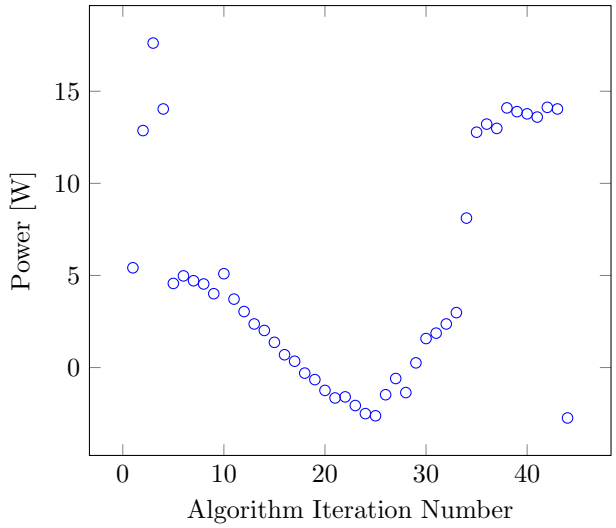

Fig. 13. Phase between coil currents and power at the receive side for each iteration of the MPP tracking algorithm using an exhaustive search between phases of $-30°$ and $180°$.

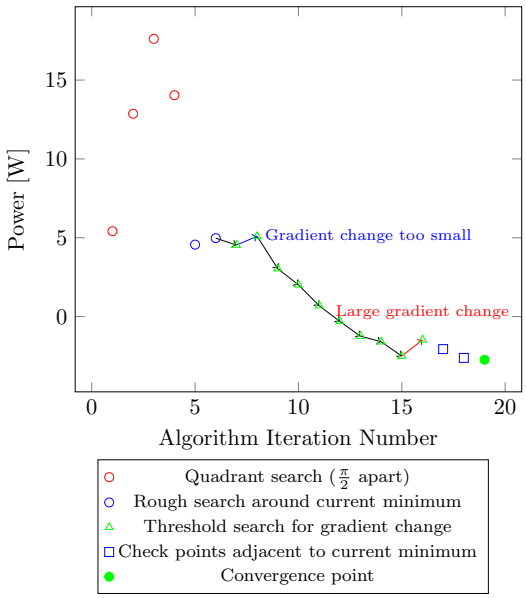

Fig. 14. Revised MPP tracking algorithm based on gradient change.

transmitter is hard-switching, carrying most of the losses of the end-to-end system, but minimising losses on the receive side.

The losses could be balanced if the system was designed to optimise for maximum efficiency, rather than using only the information on the receiver to achieve MPP tracking. This would however require additional hardware and a communication link to obtain the information from the transmitter as well, and in this work a feedback loop is implemented based exclusively on measurements of the receiver.

This work utilises a MPP tracking algorithm similar to that of [23]. A quadrant check is first performed, testing four points that are $90°$ apart from each other, and the search is subsequently narrowed down to a specific quadrant. The algorithm will then perform a fine search to track the optimal phase, which corresponds to the maximum received power (negative power indicates power is received). Operation of the algorithm is summarised in Fig. 13.

This version of the algorithm takes an average of 5.6 seconds to run, as each point is measured several times and averaged. The execution time can however be problematic, especially when the power level is large and the system is operating sub-optimally: the transmitter or the receiver could be heating up and getting damaged.

To address this issue the algorithm was modified to skip intermediate points in the narrow search, and testing the two neighbouring point of the last optimal point that has been found. A further modification is an interruption of the fine search when a positive gradient above a certain threshold is detected in the measurement. These modifications are shown

in Fig. 14. These changes, together with a decreased amount of measurement per tested point, led to a decrease of the execution time to 1.6 seconds (20 steps with an average of $80\,\mathrm{ms}$ per step). The first step is a quadrant search, testing four different points which are selected to be90° away from each other. Two points near the current optimal solution are then tested before initiating a rough search in 4° steps. This step aims to find an unambiguous change in gradient, corresponding to a local minimum. Two points near the candidate solution for local minimum are then tested to ensure convergence to the optimal phase.

With the first method an average phase error of 2° was obtained, while with the second method the average error was 5°. This can be attributed to the decreased amount of measurement time per point, together with the fact that the second method is skipping intermediate points in the fine search: when samples are not skipped, it is likely that neighboring samples will have somewhat similar values. This means that the effect of noise in a specific sample on the final convergence value is minimised by the presence of its neighbors acting as a form of extra averaging.

This issue was addressed by performing subsequent corrections after convergence at fixed time intervals of 5 seconds. In addition to bringing the error back down to 2°, these post-convergence corrections help ensure that the system is still operating under the MPP even under a change of conditions such as coupling or the introduction of foreign objects.

Another advantage of using a faster algorithm is that the effect of slow temperature changes in proximity of the oscillator circuit will have an almost negligible effect on convergence. If the algorithm was extremely slow, it is possible that the MPP tracking would be affected by a change of temperature of the environment, which could cause a change in ω_0, hence causing a drift in the phase.

This paper presents a solution which does not require a separate communication link, eliminates complicated signal processing tasks, and allows operation under extremely low coupling conditions. The auxiliary circuitry does not require any high-performance instrumentation, making it possible to be integrated in the system as a low-cost solution for active-active operation.

The closed loop system was tested in different coupling arrangements, achieving a maximum power transmission of 25.7 W for a coupling of 8.4 %, with an end-to-end efficiency of 60.9 %.

VI. Conclusion

This work shows a technique to achieve frequency and phase synchronisation of an HF-IPT system where both sides are active, enabling the possibility of synchronous and bidirectional operation.

The basic principles of injection locking are discussed and it demonstrated how this can be applied to a bidirectional HF-IPT system operating at 13.56 MHz for couplings between 1.2 % and 8.4 %, together with experimental results showing the power exchanged at each coupling.

The possibility of closed loop operation has been presented together with experimental results for a closed loop design to account for temperature variations and a MPP tracking approach to fine-tune the optimal phase.

References

[1] G. Covic, J. T. Boys *et al.*, "Modern trends in inductive power transfer for transportation applications," *IEEE Trans. Emerg. Sel. Topics Power Electron.*, vol. 1, no. 1, pp. 28–41, 2013.

[2] M. Neath, U. Madawala, and D. Thrimawithana, "Frequency jitter control of a multiple pick-up Bidirectional Inductive Power Transfer system," *Proc. IEEE Int. Conf. Ind. Technol.*, pp. 521–526, 2013.

[3] U. K. Madawala and D. J. Thrimawithana, "A bidirectional inductive power interface for electric vehicles in v2g systems," *IEEE Transactions on Industrial Electronics*, vol. 58, no. 10, pp. 4789–4796, 2011.

[4] D. J. Thrimawithana, U. K. Madawala, and M. Neath, "A synchronization technique for bidirectional ipt systems," *IEEE Transactions on Industrial Electronics*, vol. 60, no. 1, pp. 301–309, 2013.

[5] P. D. Mitcheson, D. Boyle, G. Kkelis, D. Yates, J. A. Saenz, S. Aldhaher, and E. Yeatman, "Energy-autonomous sensing systems using drones," in *2017 IEEE SENSORS*, 2017, pp. 1–3.

[6] J. Choi, D. Tsukiyama, Y. Tsuruda, and J. Rivas, "13.56 MHz 1.3 kW resonant converter with GaN FET for wireless power transfer," in *IEEE Wireless Power Transfer Conf. (WPTC)*, May 2015, pp. 1–4.

[7] M. Liu, S. Liu, and C. Ma, "A High-Efficiency/Output Power and Low-Noise Megahertz Wireless Power Transfer System Over a Wide Range of Mutual Inductance," *IEEE Trans. Microw. Theory Techn.*, vol. PP, no. 99, pp. 1–9, 2017.

[8] G. Zulauf and J. M. Rivas Davila, "Single-Turn Air-Core Coils for High-Frequency Inductive Wireless Power Transfer," *IEEE Trans. Power Electron.*, pp. 1–1, 2019.

[9] J. M. Arteaga, S. Aldhaher, G. Kkelis, D. C. Yates, and P. D. Mitcheson, "Multi-MHz IPT Systems for Variable Coupling," *IEEE Trans. Power Electron.*, vol. 33, no. 9, pp. 7744–7758, Sept 2018.

[10] A. Kurs, A. Karalis, R. Moffatt, J. D. Joannopoulos, P. Fisher, and M. Soljačić, "Wireless power transfer via strongly coupled magnetic resonances," *Science*, vol. 317, no. 5834, pp. 83–86, 2007.

[11] M. Pinuela, D. C. Yates, S. Lucyszyn, and P. D. Mitcheson, "Maximizing DC-to-Load Efficiency for Inductive Power Transfer," *IEEE Trans. Power Electron.*, vol. 28, no. 5, pp. 2437–2447, May 2013.

[12] S. Aldhaher, D. C. Yates, and P. D. Mitcheson, "Load-Independent Class E/EF Inverters and Rectifiers for MHz-Switching Applications," *IEEE Trans. Power Electron.*, pp. 1–1, 2018.

[13] W. D. Braun and D. J. Perreault, "A High-Frequency Inverter for Variable-Load Operation," *IEEE Trans. Emerg. Sel. Topics Power Electron.*, vol. 7, no. 2, pp. 706–721, 2019.

[14] A. Kumar, S. Sinha, and K. K. Afridi, "A high-frequency inverter architecture for providing variable compensation in wireless power transfer systems," in *Proc. IEEE Appl. Power Electron. Conf. Expo.*, 2018, pp. 3154–3159.

[15] Y. Han, O. Leitermann, D. A. Jackson, J. M. Rivas, and D. J. Perreault, "Resistance Compression Networks for Radio-Frequency Power Conversion," *IEEE Trans. Power Electron.*, vol. 22, no. 1, pp. 41–53, 2007.

[16] G. Kkelis, D. C. Yates, and P. D. Mitcheson, "Class-E Half-Wave Zero dv/dt Rectifiers for Inductive Power Transfer," *IEEE Trans. Power Electron.*, vol. 32, no. 11, pp. 8322–8337, Nov 2017.

[17] K. Li, S. Tan, and R. S. Y. Hui, "Single-Switch-Regulated Resonant WPT Receiver," *IEEE Trans. Power Electron.*, vol. 34, no. 11, pp. 10 386–10 391, 2019.

[18] N. Pucci, J. M. Arteaga, and P. D. Mitcheson, "Dynamic receiver characterisation in hf-ipt systems," in *2022 Wireless Power Week (WPW)*, 2022, pp. 308–312.

[19] J. M. Arteaga, L. Lan, C. H. Kwan, D. C. Yates, and P. D. Mitcheson, "Characterisation of high frequency inductive power transfer receivers using pattern recognition on the transmit side waveforms," in *2020 IEEE Applied Power Electronics Conference and Exposition (APEC)*, 2020, pp. 825–831.

[20] X. Zan and A.-T. Avestruz, "Performance comparisons of synchronous and uncontrolled rectifiers for 27.12 mhz wireless power transfer using cmcd converters," in *2018 IEEE Energy Conversion Congress and Exposition (ECCE)*, 2018, pp. 2448–2455.

[21] E. Asa, K. Colak, M. Bojarski, and D. Czarkowski, "A novel phase control of semi bridgeless active rectifier for wireless power transfer applications," in *Proc. IEEE Appl. Power Electron. Conf. Expo.*, 2015, pp. 3225–3231.

[22] S. Cochran and D. Costinett, "Frequency Synchronization and Control for a 6.78 MHz WPT Active Rectifier," in *Proc. IEEE 19th Workshop Control Model. Power Electron.*, 2018, pp. 1–7.

[23] N. Pucci, J. M. Arteaga, C. H. Kwan, D. C. Yates, and P. D. Mitcheson, "A 13.56 mhz bidirectional ipt system with wirelessly synchronised transceivers for ultra-low coupling operation," in *2021 IEEE Energy Conversion Congress and Exposition (ECCE)*, 2021, pp. 5781–5787.

[24] Z. Kaczmarczyk, "High-Efficiency Class E, EF_2 , and E/F_3 Inverters," *IEEE Trans. Ind. Electron*, vol. 53, no. 5, pp. 1584–1593, Oct 2006.

[25] N. Pucci, J. M. Arteaga, and P. D. Mitcheson, "Design and development of a test rig for 13.56 mhz ipt systems with synchronous rectification and bidirectional capability," in *Proc. IEEE PELS Workshop Emerg. Technol.*, 2021, pp. 1–5.

[26] E. Skountzos, J. M. Arteaga, E. Hadjittofis, D. C. Yates, K. L. Sedransk Campbell, and P. D. Mitcheson, "A 13.56 mhz inductive power transfer system operating with corroded coils," in *2019 IEEE PELS Workshop on Emerging Technologies: Wireless Power Transfer (WoW)*, 2019, pp. 335–340.

[27] R. Adler, "A study of locking phenomena in oscillators," *Proceedings of the IRE*, vol. 34, no. 6, pp. 351–357, 1946.

[28] L. Paciorek, "Injection locking of oscillators," *Proceedings of the IEEE*, vol. 53, no. 11, pp. 1723–1727, 1965.

[29] B. Razavi, "A study of injection locking and pulling in oscillators," *IEEE Journal of Solid-State Circuits*, vol. 39, no. 9, pp. 1415–1424, 2004.

[30] B. Hong and A. Hajimiri, "A general theory of injection locking and pulling in electrical oscillators—part i: Time-synchronous modeling and injection waveform design," *IEEE Journal of Solid-State Circuits*, vol. 54, no. 8, pp. 2109–2121, 2019.

[31] ——, "A general theory of injection locking and pulling in electrical oscillators—part ii: Amplitude modulation in lc oscillators, transient behavior, and frequency division," *IEEE Journal of Solid-State Circuits*, vol. 54, no. 8, pp. 2122–2139, 2019.

[32] J. M. Arteaga, L. Lan, S. Aldhaher, G. Kkelis, D. C. Yates, and P. D. Mitcheson, "A multi-mhz ipt-link developed for load characterisation at highly variable coupling factor," in *2018 IEEE Wireless Power Transfer Conference (WPTC)*, 2018, pp. 1–4.

[33] G. Feng and J.-J. Sit, "An injection-locked wireless power transfer transmitter with automatic maximum efficiency tracking," *IEEE Transactions on Industrial Electronics*, vol. 68, no. 7, pp. 5733–5743, 2021.

[34] N. Pucci, J. M. Arteaga, C. H. Kwan, D. C. Yates, and P. D. Mitcheson, "Induced voltage estimation from class ef switching harmonics in hf-ipt systems," *IEEE Transactions on Power Electronics*, vol. 37, no. 4, pp. 4903–4916, 2022.